An investigation into the grindability of additively manufactured 42CrMo4 steel

CIRP Annals - Manufacturing Technology 73 (2024) 257–260

Contents lists available at ScienceDirect

CIRP Annals - Manufacturing Technology

journal homepage: https://www.editorialmanager.com/CIRP/default.aspx

An investigation into the grindability of additively manufactured 42CrMo4 steel

Philipp Hoier[a], Deepa Kareepadath Santhosh[b], Eduard Hryha[a], Peter Krajnik (2)[a,*]

[a] Department of Industrial and Materials Science, Chalmers University of Technology, Gothenburg, Sweden
[b] Faculty of Mechanical Engineering, University of Ljubljana, Ljubljana, Slovenia

ARTICLE INFO

Article history:
Available online 26 April 2024

Keywords:
Grinding
Grindability
Additive manufacturing

ABSTRACT

This study investigates post-processing of additively manufactured (AM) low-alloy 42CrMo4 steel (AISI 4140) produced by powder bed fusion – laser beam (PBF-LB). While the PBF-LB process produces tempered martensite by in-situ heat-treatment, resulting in superior mechanical properties, finishing by grinding remains critical for use in precision components such as automotive gears. The grindability of the AM material is compared to conventionally produced steel and reveals comparable results to most of the grindability criteria tested. However, higher wheel wear is observed when grinding the AM material. This is likely due to the lack of machinability-enhancing inclusion treatment common in conventional steelmaking.

1. Introduction

The fabrication of precision components by depositing material layer-by-layer instead of by conventional material-conversion processes (e.g., forming and casting) and/or material-removal (subtractive) processes offers advantages such as near-net shape material conversion and minimizing/avoiding machining – enabling a more flexible production chain [1]. While the increased precision of metal additive manufacturing (AM) in recent years reduced the required amount of post-processing [2] to meet dimensional tolerance, the requirements for functional surfaces necessitate a well-understood post-processing, ranging from machining [3–5] to finishing [6–9]. Despite the importance of grinding as a surface-finishing post-processing operation, only a few studies have been dedicated to investigating grindability of AM materials. Recent investigations include diamond grinding of AM SiC [10], micro grinding of Ti6Al4V produced by powder-based fusion using electron beam (PBF-EB) [11], grinding of Ni-based superalloys [12] and austenitic stainless steels [13,14], both produced by powder-based fusion using a laser-based system (PBF-LB) and using direct-energy deposition [15].

Kirsch et al. compared the grindability of conventional stainless steel (cast, rolled, annealed, and quenched) with PBF-LB-produced steel that had varying defect sizes and densities [13]. The grindability assessment included measuring grinding forces and surface roughness. In pendulum-grinding mode, the dense AM material exhibited about 40 % higher specific tangential force than conventional steel, which was attributed to the difference in hardness. However, in creep-feed mode, the forces were similar, indicating that hardness alone cannot fully explain the differences in grindability. Pendulum grinding revealed the influence of microstructural features such as defects and material texture. The results for surface roughness were comparable. However, larger cracks and voids observed on the ground surfaces of AM materials indicated that the achievable finish is influenced by residual porosity. This porosity is independent of the grinding method and is linked to the material density.

Another study provided comprehensive insights into surface integrity and mechanical properties of ground 304 L stainless steel processed by PBF-LB [14]. Here material anisotropy and microstructural heterogeneity were regarded as the main factors affecting the grindability. Grinding improved surface quality and fatigue life by removing “lack-of-fusion” defects near the as-built surface.

This study builds upon a successful development of PBF-LB process for fabricating 42CrMo4 steel (AISI 4140) – achieving microstructural and mechanical properties (defect-free with a fine, martensitic microstructure with high density, > 99.8 %) superior to those of the conventionally-produced material. Specifically superior tensile strength, impact toughness, and elongation exceeding ASTM standards were reported [16]. Another advantage of the PBF-LB process is its in-situ heat treatment of the material yielding tempered martensite directly in as-printed state. This is especially attractive since it potentially eliminates the need for additional hardening and tempering [16]. This indicates that the AM material in focus here is not only suitable, but also takes full advantage of PBF-LB to achieve properties that meet or exceed those of conventionally-produced alloys. This process is therefore potentially suitable for 3D-printing of precision components such as automotive gears, which, however, require grinding to meet the quality demands for functional surfaces.

Although the manufacturing community has started to address grindability of AM materials, available research is limited to a few materials, namely stainless steels and Ti-/Ni-based alloys. Structural low-alloy steels in hardened conditions have not been studied so far. In addition, previous studies focused on AM materials with anisotropic microstructures and with printing defects. Defect-free materials with limited anisotropic properties due to small grains with limited crystallographic texture as reported for the alloy investigated

* Corresponding author.
E-mail address: krajnik@chalmers.se (P. Krajnik).

https://doi.org/10.1016/j.cirp.2024.04.039

here [16] have not been addressed so far. Therefore, this research aims to address a significant gap in the available research on the grindability of low-alloy structural steel fabricated by AM.

2. Experimental

PBF-LB was carried out using an EOS M290 machine equipped with a Yb-fibre laser. Pre-alloyed, inert-gas atomized powder supplied by Sandvik Osprey™ was used as the feedstock 42CrMo4 material. The $10 \times 35 \times 100$ mm^{3}AM blanks were printed using constant laser power (170 W), hatch spacing (0.07 mm), layer thickness (0.02 mm) and laser speed (1012 mm/s). During laser exposure, a 5 mm stripe scan pattern, a 0.003 mm hatch offset, and a 67° scan rotation angle were used. During processing, an oxygen level of ~0.1 % was maintained within the building chamber using Argon gas. The AM material did not undergo any additional heat treatment. Its top surface exhibited a layer of hard, untempered martensite approximately 100 µm deep, as previously reported by Hearn et al. [17]. This layer was removed prior to grinding tests to ensure homogeneous microstructure and consistent test conditions. The conventional material was quenched and tempered – with rolling direction perpendicular to the grinding direction (see Fig. 1).

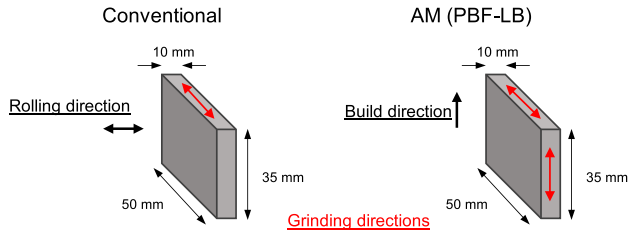

Fig. 1. Schematic of workpieces used for the grinding tests with relationship between grinding, building, and rolling directions.

Grinding tests were performed on a Blohm Planomat HP 408 surface grinder using a synthetic grinding fluid (Quakercool 2920 EVC) at 8 % concentration. A Norton Quantum Prime grinding wheel (5NQNX60H16VS3X, diameter $d_s = 400$ mm, width $b_s = 30$ mm) was used. Single-point dressing was employed with dressing depth $a_d = 0.025$ mm and dressing overlap ratio $U_d = 5.4$.

Workpieces were mounted on a dynamometer (Kistler 9139AA) which was fixed onto the machine table. It measured the normal F_n and tangential F_t forces for six different workpiece speeds v_w (Table 1) at constant wheel speed $v_s = 30$ m/s, depth of cut $a_e = 0.01$ mm, and active grinding wheel width $b_d = 10$ mm. For each test, the arithmetic mean of the forces from three grinding passes was determined. Based on these results, the specific energy was calculated as:

$$e_G = \frac{F_t \cdot v_s}{v_w \cdot a_e \cdot b_d} \quad (1)$$

The grinding parameters (Table 1) were varied to obtain different aggressiveness numbers [18] calculated by:

$$Aggr = \left(\frac{v_w}{v_s}\right)\sqrt{\frac{a_e}{d_s}} \quad (2)$$

Table 1
Workpiece speeds used to obtain six different levels of grinding aggressiveness typical for: finishing ($Aggr = 1.7 - 16.7$), semi-finishing ($Aggr = 16.7 - 50$), and rough grinding ($Aggr = 50 - 111.1$).

Condition	1	2	3	4	5	6
Aggr	1.7	8.3	16.7	50.0	83.3	111.1
v_w [mm/s]	10	50	100	300	500	667

For the analysis of the workpieces' compositions, samples were analyzed using X-ray spectrometry, optical emission spectrometry, and combustion analysis. Microstructural inspection included etching of metallographic samples using Nital (2 %) and imaging using light optical (LOM) and electron microscopy (SEM). Post-test analysis of surface integrity comprised residual stress measurements using a diffractometer with a CrKα X-ray source (30 kV, 9 mA) and use of the modified $\sin^2\chi$ method. Stepwise electrochemical etching was used to obtain stress depth profiles.

3. Results and discussion

3.1. Material characterization

The chemical analyses of the workpieces are summarized in Table 2. The printed AM material exhibits a notably higher oxygen (O) content due to oxide layers on feedstock powders, which have a much larger surface area compared to equivalent bulk material [19]. The conventional material, however, contains higher levels of sulfur (S), copper (Cu) and calcium (Ca). Higher levels of sulfur and calcium indicate efforts to machinability/grindability enhancements by inclusion control via Ca-treatment and introduction of sulfides during the conventional steelmaking process. Higher levels of copper likely stem from recycling.

Table 2
Composition (in wt.%) of the 42CrMo4 workpieces fabricated via conventional route and AM.

	C[a]	Si[b]	Mn[b]	P[c]	S[a]	Cr[b]
Conv.	0.403	0.29	0.81	0.006	0.030	0.96
AM	0.348	0.39	0.78	0.012	0.006	1.00
	Ni[b]	**Cu[b]**	**Co[b]**	**Mo[b]**	**Ca[c]**	**O[a]**
Conv.	0.20	0.18	0.015	0.16	0.0032	0.0017
AM	0.14	0.038	0.011	0.24	<0.0005	0.0127

Analysis techniques.
[a] Combustion analysis.
[b] X-ray spectrometry.
[c] Optical emission spectrometry.

Before grinding, workpieces underwent characterization to determine their initial hardness and microstructure (see Fig. 2). The conventional material contained a tempered martensitic microstructure with some banding along the rolling direction. The average Vickers hardness was 299 ± 16 HV1. In contrast, the AM-material contained finer tempered martensite (see Fig. 2b). Its average Vickers hardness was 437 ± 13 HV1, i.e. approximately 46 % greater than that of its conventionally produced counterpart.

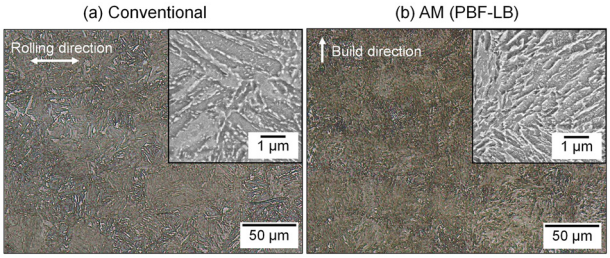

Fig. 2. LOM and SEM (high magnification inserts) micrographs of conventional and AM material.

Polished samples (without etching) were examined using SEM with backscattered electron imaging and energy-dispersive X-ray spectroscopy to identify non-metallic inclusions. The conventional material contained elongated MnS inclusions that were aligned with the rolling direction and presence of oxide particles (see examples in Fig. 3a). In contrast, the AM-produced material exhibited no MnS particles due to the lack of significant amounts of sulfur in that material (Table 2). Instead, this material only contained spherical oxide inclusions (Fig. 3b). The composition of oxide inclusions in the tested materials differed, with the conventional material featuring traces of Ca (due to Ca-treatment), while the AM material's oxides did not have these characteristics according to EDS analyses.

Sulfide inclusions are generally considered to have favorable properties for the grindability/machinability of materials as they provide a lubricating effect and reduce friction and wear on tools. In contrast, the abrasiveness of hard oxide inclusions tends to negatively

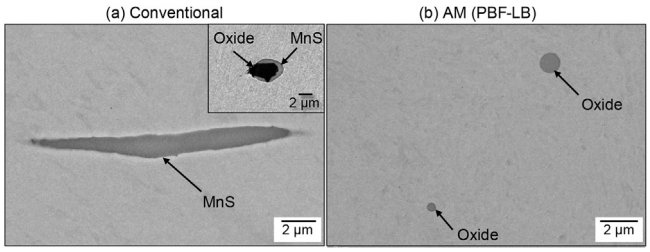

Fig. 3. MnS and oxide inclusions in the conventional material and oxide inclusions in AM-produced material.

impact tool wear [2,20]. However, the hardness of oxide inclusions can be reduced through Ca-treatment [21]. Hence, the non-metallic inclusions present in the AM material differ from those found in the conventionally-produced material in terms of type and resulting properties. This difference may affect the wear of the grinding wheel. Based on the preceding discussion, it appears that the inclusions in the AM material are disadvantageous compared with the inclusions in the conventional material.

3.2. Grindability testing

Grindability is a term to describe the ease of grinding a work material using a specific combination of abrasive and grinding conditions. This work evaluated grindability based on the following criteria:

- Mechanical: Specific grinding energy and forces (relating to material flow stress, strain, strain rate, hardness, etc.);
- Tribological: Force ratio and wheel wear (relating to work material microstructures, non-metallic inclusions);
- Surface integrity: Surface roughness and residual stresses (relating to thermo-mechanical effects).

The first set of tests shown in Fig. 4 was aimed at comparing the grindability independent of the effect of changing wheel topography due to wheel wear. For this purpose, the wheel was dressed prior to each test followed by grinding just enough material to overcome the initial transient behavior of the freshly dressed wheel and to reach a steady grinding condition. The specific grinding energy curves are shown in Fig. 4a. Materials with low specific grinding energy are easier to grind than those with high specific energy, meaning they have better grindability. Here, the measured specific energies for grinding both materials were similar with a slight trend of lower values for the AM material (differences below 7 %). The grinding direction in relation to the build direction shows no influence on the resulting specific energy. Typically, anisotropic properties of AM materials tend to result in an anisotropic response during post-processing [2]. Such effects are unlikely to have been observed here since the material has very limited crystallographic texture and anisotropic properties, as investigated by Hearn et al. [16].

Similar specific grinding energies are noteworthy considering the differences in average hardness of the workpieces. However, hardness alone does not fully capture how a material behaves during grinding; factors such as strain hardening and elongation to fracture can play a substantial role and influence the forces.

The surface finish was evaluated based on the arithmetic mean-height roughness *Ra*, see Fig. 4b. At lower grinding aggressiveness, roughness values were all similar. At higher aggressiveness, the AM-materials resulted in slightly lower *Ra* values. The differences are small and there is often experimental scatter in roughness measurements.

Fig. 5 shows the grinding forces and the grinding force ratio $\mu = F_t / F_n$ for conventional and AM materials as material-removal progressed (no re-dressing). Both materials showed the typical initial decrease in forces (due to wheel break-in) followed by a slow but steady increase in normal and tangential forces. While the increase in tangential forces is slight, the normal forces increase relatively more as the grinding progresses.

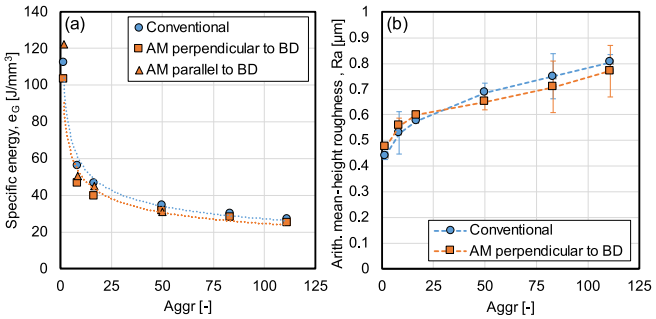

Fig. 4. Specific grinding energy e_g and arithmetic mean-height roughness *Ra* vs. aggressiveness number *Aggr*. Error bars show the ranges of the three measurements.

When comparing the two materials, it is apparent that the forces increase more rapidly for the AM material, this is especially pronounced for the normal force.

The pronounced increase in normal force suggests a progression of wear at the grit level causing dulling and a gradual increase in the wheel/workpiece contact area. This effect appears to be more pronounced for the AM material (higher normal forces for AM material), suggesting a higher rate of wheel wear. Grit dulling is also suggested in Fig. 5b where comparatively lower force ratios as grinding time progresses indicate gradual dulling of the grinding wheel [22], again this effect is more pronounced for the AM material.

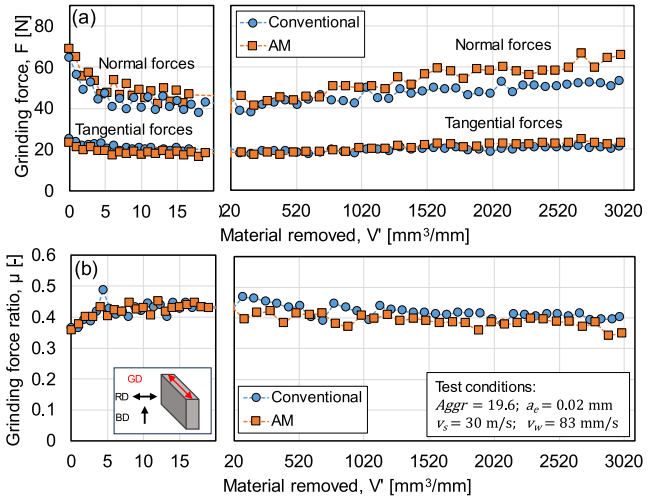

Fig. 5. Normal (F_n) and tangential (F_t) grinding forces and grinding-force ratio μ vs amount of material ground per mm width of grinding wheel. Grinding (GD), rolling (RD), and build direction (BD) are indicated.

Wheel wear was also quantified using the G-ratio, which is the volume of material ground away divided by the volume of wheel worn away. Measurements of wheel wear were performed using the razor-blade technique after the grinding tests shown in Fig. 5. The conventional material had a G-ratio of 500, while the AM-produced material had a G-ratio of 388, indicating that grinding of the AM material results in almost 30 % higher wheel wear. This result is consistent with the F_n, F_t, and μ measurements (see Fig. 5). Both suggest lower grindability (i.e., more wheel wear) in the case of AM material. These differences are likely the results of the inclusion characteristics outlined earlier (Fig. 3), which indicated comparably unfavorable inclusion properties for the AM material.

In contrast, differences in bulk workpiece hardnesses are unlikely to have significantly affected wheel wear, given the similar specific energies for both materials (i.e. similar forces on the grits). Furthermore, the relatively low hardness of the steel matrix (tempered martensite) compared to the Al_2O_3 grits minimizes its potential for attritious (abrasive) wheel wear.

The impact of inclusions on tool wear was also observed when machining with geometrically defined cutting edges where it has

been established that sulfur-induced manganese sulfide (MnS) inclusions have lubricating effects [2,21]. Moreover, oxide inclusions softened through modification by Ca-treatment are reported to reduce tool wear [21]. Such modified inclusions may also form protective layers on the tool surface, acting as diffusion barriers and mitigating tool wear [23]. A combination of some of these effects may contribute to the lower wear in grinding the conventional material.

Fig. 6 shows the residual stress profiles after grinding under finishing ($Aggr = 1.7$) and rough-grinding conditions ($Aggr = 111.1$). Surface stresses for finishing are compressive for both materials. However, the compressive stress for AM material shifts to tensile at about 0.2 mm below the surface, while the conventional material reaches stress-free state. The presence of internal residual stress in the AM material is typical for such as-built components and is associated with the thermal history and temperature gradients during the AM process [2]. Finish grinding notably shifts the AM material's stress from tensile to compressive. This is likely the result of mechanical effects (plastic deformation during chip formation, plowing, and rubbing) that govern residual stress development. Such compressive residual stresses are favored as they enhance the fatigue properties of components [24]. In contrast, rough grinding yielded tensile surface stresses in both materials, with thermal effects dominating the development of residual stress. It is important to note also that inherent residual stresses present in AM-produced material can be relieved, but this requires the development of a tailored heat treatment.

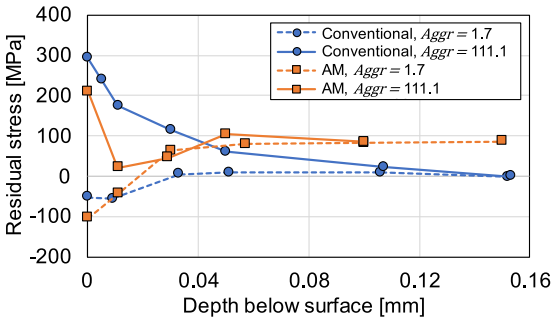

Fig. 6. Depth profiles of residual stresses parallel to grinding direction.

4. Conclusions

This study addresses the research gap in grinding as a post-processing finishing operation for additively manufactured (AM) low-alloy structural steel, with a focus on steel produced by powder bed fusion - laser beam (PBF-LB). The grindability of this steel was investigated and compared to that of conventionallyproduced material. Despite differences in microstructure and mechanical properties, the characteristics of the grinding process were comparable in terms of most of the tested grindability assessment criteria, such as specific grinding energy and surface integrity. However, the AM material had poorer grindability in terms of wheel wear due to unfavorable inclusion properties. Grinding-process adaptations, such as adjusting dressing intervals to accommodate varying wheel-wear rates, may be necessary. Nevertheless, grinding is a viable post-process for finishing PBF-LB low-alloy structural steels. Future work will investigate surface modifications and thermal treatments to examine how martensite characteristics and grain size affect grindability as well as fatigue life, focusing on applications such as gear grinding.

Declaration of competing interest

The authors declare that they have no known competing financial interests or personal relationships that could have appeared to influence the work reported in this paper.

CRediT authorship contribution statement

Philipp Hoier: Conceptualization, Formal analysis, Investigation, Methodology, Project administration, Supervision, Visualization, Writing – original draft, Writing – review & editing. **Deepa Kareepadath Santhosh:** Formal analysis, Investigation, Methodology, Visualization. **Eduard Hryha:** Conceptualization, Funding acquisition, Resources, Writing – review & editing. **Peter Krajnik:** Conceptualization, Funding acquisition, Project administration, Resources, Supervision, Writing – original draft, Writing – review & editing.

Acknowledgements

The authors thank William Hearn for support and Saint-Gobain Abrasives for sponsoring this research. Lutz Gaida and Anders Smith were particularly supportive. The project was carried out under the umbrella of the IGC competence network belonging to Chalmers Centre for Metal Cutting Research (MCR) and Centre for Additive Manufacture – Metal (CAM^2).

References

[1] Krajnik P, Hashimoto F, Karpuschewski B, Da Silva EJ, Axinte D (2021) Grinding and fine finishing of future automotive powertrain components. *CIRP Ann* 70:589–610.
[2] Malakizadi A, Mallipeddi D, Dadbakhsh S, M'Saoubi R, Krajnik P (2022) Post-processing of additively manufactured metallic alloys – A review. *Int J Mach Tools Manuf* 179:103908.
[3] Bertolini R., Bruschi S., Ghiotti A., Savio E., Ceseracciu L., Jawahir IS, 2023, Surface integrity and superelastic response of additively manufactured Nitinol after heat treatment and finish machining, CIRP Ann, 72:501–4.
[4] Kishawy HA, Nguyen N, Hosseini A, Elbestawi M (2023) Machining characteristics of additively manufactured titanium, cutting mechanics and chip morphology. *CIRP Ann* 72:49–52.
[5] Malakizadi A, Hajali T, Schulz F, Cedergren S, Ålgårdh J, M'Saoubi R, et al. (2021) The role of microstructural characteristics of additively manufactured Alloy 718 on tool wear in machining. *Int J Mach Tools Manuf* 171:103814.
[6] Rotella G., Filice L., Micari F. Improving surface integrity of additively manufactured GP1 stainless steel by roller burnishing 2020, CIRP Ann, 69:513–6.
[7] Sealy MP, Karunakaran R, Ortgies S, Madireddy G, Malshe AP, Rajurkar KP (2021) Reducing corrosion of additive manufactured magnesium alloys by interlayer ultrasonic peening. *CIRP Ann* 70:179–182.
[8] Shinonaga T, Yamaguchi A, Okamoto Y, Okada A (2021) Surface smoothing and repairing of additively manufactured metal products by large-area electron beam irradiation. *CIRP Ann* 70:143–146.
[9] Wang B, Castellana J, Melkote SN (2021) A hybrid post-processing method for improving the surface quality of additively manufactured metal parts. *CIRP Ann* 70:175–178.
[10] Horvath N, Honeycutt A, Davies MA (2020) Grinding of additively manufactured silicon carbide surfaces for optical applications. *CIRP Ann* 69:509–512.
[11] Kadivar M, Azarhoushang B, Klement U, Krajnik P (2021) The role of specific energy in micro-grinding of titanium alloy. *Precis Eng* 72:172–183.
[12] Liu Z, Li X, Wang X, Tian C, Wang L (2019) Comparative investigation on grindability of Inconel 718 made by selective laser melting (SLM) and casting. *Int J Adv Manuf Technol* 100:3155–3166.
[13] Kirsch B, Hotz H, Hartig J, Greco S, Zimmermann M, Aurich JC (2021) Pendulum and creep feed grinding of additively manufactured AISI 316L. *Procedia CIRP* 101:166–169.
[14] Zhang H, Li C, Yao G, Shi Y, Zhang Y (2022) Investigation of surface quality, microstructure, deformation mechanism, and fatigue performance of additively manufactured 304L stainless steel using grinding. *Int J Fatigue* 160:106838.
[15] Souza AM, Silva EJD, Yamaguchi H (2023) Effects of post-processing operations on directed energy deposited 316L stainless steel surfaces. *Int J Adv Manuf Technol* 129:2087–2109.
[16] Hearn W, Harlin P, Hryha E (2022) Development of powder bed fusion – laser beam process for AISI 4140, 4340 and 8620 low-alloy steel. *Powder Metall* : 1–13.
[17] Hearn W, Steinlechner R, Hryha E (2022) Laser-based powder bed fusion of non-weldable low-alloy steels. *Powder Metall* 65:121–132.
[18] Badger J, Dražumerič R, Krajnik P (2021) Application of the dimensionless aggressiveness number in abrasive processes. *Procedia CIRP* 102:361–368.
[19] Hryha E, Shvab R, Gruber H, Leicht A, Nyborg L (2018) Surface oxide state on metal powder and its changes during additive manufacturing: an overview. *La Metallurgia Italiana* 3:34–39.
[20] Badger J (2007) Grindability of conventionally produced and powder-metallurgy high-speed steel. *CIRP Ann* 56:353–356.
[21] Ånmark N, Karasev A, Jönsson P (2014) The effect of different non-metallic inclusions on the machinability of steels. *Materials* 8:751–783.
[22] Rowe WB (2014) *Basic Material Removal, Principles of Modern Grinding Technology*, Elsevier, 15–33.
[23] Hoier P, Malakizadi A, Friebe S, Klement U, Krajnik P (2019) Microstructural variations in 316L austenitic stainless steel and their influence on tool wear in machining. *Wear* 428–429:315–327.
[24] La Monaca A, Murray JW, Liao Z, Speidel A, Robles-Linares JA, Axinte DA, et al. (2021) Surface integrity in metal machining - Part II: functional performance. *Int J Mach Tools Manuf* 164:103718.